Taylor & Francis
Taylor & Francis Group

Vehicle System Dynamics
International Journal of Vehicle Mechanics and Mobility

ISSN: (Print) (Online) Journal homepage: https://www.tandfonline.com/loi/nvsd20

Estimation of the trajectory and attitude of railway vehicles using inertial sensors with application to track geometry measurement

J. González-Carbajal, Pedro Urda, Sergio Muñoz & José L. Escalona

To cite this article: J. González-Carbajal, Pedro Urda, Sergio Muñoz & José L. Escalona (2023): Estimation of the trajectory and attitude of railway vehicles using inertial sensors with application to track geometry measurement, Vehicle System Dynamics, DOI: 10.1080/00423114.2023.2203865

To link to this article: https://doi.org/10.1080/00423114.2023.2203865

VEHICLE SYSTEM DYNAMICS
https://doi.org/10.1080/00423114.2023.2203865

Estimation of the trajectory and attitude of railway vehicles using inertial sensors with application to track geometry measurement

J. González-Carbajal[a], Pedro Urda[a], Sergio Muñoz[b] and José L. Escalona[a]

[a]Department of Mechanical and Manufacturing Engineering, University of Seville, Seville, Spain;
[b]Department of Materials and Transportation Engineering, University of Seville, Seville, Spain

ABSTRACT

This paper describes a novel method for the estimation of the trajectory and orientation of a rigid body moving along a railway track. Compared to other recent developments in the literature, the presented approach has the significant advantage of using inertial sensors only, excluding global position and orientation sensors. The excluded sensors are compensated with an odometry system and previous knowledge of the design track geometry. The procedure is based on a kinematic model of the relative motion of the body with respect to the track, together with a Kalman filter algorithm. Two different approaches are used and compared for the estimation of the noise covariance matrices in the Kalman filter. One is based on the use of experimental results with a known output. The other one relies upon *constrained maximum likelihood estimation*. The calculated trajectory and orientation are applied in this research to the problem of track geometry measurement. A scale track is used for experimental validation, showing that results are sufficiently accurate for this application. The obtained results also reveal that the constrained maximum likelihood estimation performs similarly to the known-output method. This is very convenient because it allows a straightforward application of the algorithm in different scenarios.

ARTICLE HISTORY
Received 6 July 2022
Revised 15 March 2023
Accepted 31 March 2023

KEYWORDS
Rail vehicles; track irregularities; multibody dynamics; inertial sensors; computer vision

1. Introduction

The problem of finding the trajectory of a body in space using inertial sensors is a classic problem that has been treated by many scientists in the fields of inertial navigation of vehicles, robotics or biomechanics. In fact, the first application of the Kalman filter in the 1960s of the last century was the inertial navigation of spacecrafts in the Apollo project. The inherent difficulty of this type of estimation is associated with the drift of the trajectory coordinates obtained by integrating acceleration and angular velocity signals that include noise. This problem can be fixed including new sensors that provide signals proportional to the trajectory coordinates themselves, not their derivatives. To this end, the most popular technology is the *global navigation satellite system* (GNSS).

CONTACT J. González-Carbajal jgcarbajal@us.es

Nowadays there exist numerous algorithms for inertial navigation that work reasonably well in many applications. The use of *state observers* aims to determine the state of the system, which may include the sensors biases [1–3] or the error parameters of the *inertial measurement unit* (IMU) [4]. *Sensor fusion algorithms* lead to estimated trajectory and orientation without the drift problem [5–11]. *Optimisation algorithms* have been successfully applied to the trajectory estimation of aircrafts, spacecrafts, cars, robots or humans. This minimisation can be approached by different algorithms such as the Levenberg–Marquardt algorithm [12], Gauss-Newton algorithm, gradient descent algorithm [13,14] and control loop [15,16]. The estimation of the trajectory of an aircraft in space is much more difficult than the estimation of the trajectory of a vehicle along a rail track. However, when the latter is used for rail geometry measurement, the accuracy that is needed is millimetric. This is much more than the accuracy required for the inertial navigation of aircrafts and other vehicles. It is apparent that new specific navigation methods must be developed for railway vehicles. This paper treats the problem of the trajectory estimation of railways with application to track geometry measurement.

In the railway industry, track geometry measurement is a fundamental phase of track maintenance. Two different types of equipment are used for this task: man-driven *rail track trolleys* (RTTs) and *track recording vehicles* (TRVs). On one hand, the technology behind the RTT is simple and accurate. The relative irregularities (track gauge and cross-level) are directly measured with a distance sensor, like a *linear variable differential transformer* (LVDT), and an inclinometer, respectively. The absolute irregularities (alignment and vertical profile) require an absolute positioning system, like a total station or a very accurate GNSS. Despite their precision and good performance, in addition to their low cost, the main handicap of RTT devices is their slowness when measuring the track. On the other hand, the technology used in TRV is more varied. Essentially, there are two technologies [17]: versine measurement systems (VMSs) and inertial measurement systems (IMSs). The VMS, also called chord method, are based on simple kinematics that only requires the measurements of distance sensors, obtaining both horizontal and vertical measurement of rails [18]. The IMS are based on the use of inertial sensors (accelerometers and gyroscopes), the most serious problem being the need to integrate the sensor signals in time to get the irregularities. Many IMS include optical sensors in addition to the inertial sensors, as does the system developed by the authors and used in this paper [19]. In contrast to other methods used in the industry, our method for using inertial and optical sensors data is fully documented. Being not very detailed, Ref. [20] is the best description about this data fusion technique that has been found in the scientific literature. The main drawback of the TRV methods is that they are based on the use of expensive and dedicated vehicles.

The alternative to both measuring methods (RTT and TRV) is the use of inexpensive measuring systems, mounted on in-service vehicles for continuous monitoring of track conditions (see Ref. [21] for an extensive review). Weston et al. published a set of papers [22,23], showing the measurement of vertical and lateral track irregularities using accelerometers and gyroscopes mounted in the bogie frame and a very simple kinematic model of the vehicle motion. Seok Lee et al. [24] presented a Kalman filter data fusion approach based on accelerometer signals mounted on the body frame (BF) and the axlebox. Wei et al. [25] proposed a method to estimate the alignment of the track through a double integration of the acceleration measured by several accelerometers placed on the

vehicle. Tsai et al. [26,27] presented a fast inspection technique based on the application of the Hilbert–Huang transform to the signal of an accelerometer mounted on the axle-box of an in-service car. Tsunashima et al. [28] estimated the vertical track geometry using the accelerations measured in the car body of the Japanese Shinkansen using a Kalman filter based on a very basic car model. More recently, De Rosa et al. [29] proposed a set of different model-based methods to estimate both lateral track alignment and cross-level irregularities. In Ref. [30], Muñoz et al. proposed a Kalman filter model-based methodology for the estimation of lateral track irregularities from measurements from different sensors mounted on an in-service vehicle. In the work of Escalona et al. [19], a track measurement system that can be installed on in-service vehicles and combines a kinematic model, a computational vision system and inertial measurement was presented. Many methodologies for track geometry measurement require the estimation of the trajectory for the measurement of the absolute irregularities. In the present work, a new method for the estimation of the trajectory and orientation of a rigid body is presented, with application to track geometry measurement. This paper is organised as follows. Section 2 presents the kinematic description of the geometry of a track, of a vehicle running on the track and their relationship with the measurements of inertial sensors. Section 3 explains the Kalman filter used to estimate the trajectory and attitude of a body moving along the track. Section 4 shows two different methods that can be used to find the covariance matrices needed for the application of the Kalman filter. Section 5 describes the experiments used for the application of the developed estimation techniques to the geometry measurement of a scale track. Section 6 shows and discusses the validity of the estimation techniques based on the assessment of the experimental results. Finally, summary and conclusions of this work are given in Section 7.

2. Kinematic models

This section shows the kinematic models used in the estimation of the trajectory and orientation of a body moving along a rail track. It is a summary of the more detailed kinematic description given in Ref. [19].

Figure 1 shows an arbitrary rigid body b that moves along a rail track. The track is represented by its centreline and its horizontal projection to the plane $Z = 0$. This projection is important in railway kinematics because the arc-length coordinate s is defined along this curve and its tangent vector is used to define the heading angle of the track, as shown in the figure. The figure shows three frames: (1) an inertial and *global frame* (GF) $< X, Y, Z >$ that is fixed in space, (2) a *track frame* (TF) $< X^t, Y^t, Z^t >$ whose position and orientation are known functions of the arc-length coordinate along the track s and (3) the *BF* $< X^b, Y^b, Z^b >$ that is rigidly attached to the body.

2.1. Kinematics of the track centreline

Describing the kinematics of the track centreline is equivalent to providing the functions that give the position and orientation of the TF with respect to the GF. The definition of the TF is such that the X^t axis is tangent to the track design centreline, the Y^t axis is perpendicular to X^t and connects the left rail centreline and the right rail centreline and the Z^t axis is perpendicular to both X^t and Y^t. The components of the absolute position vector

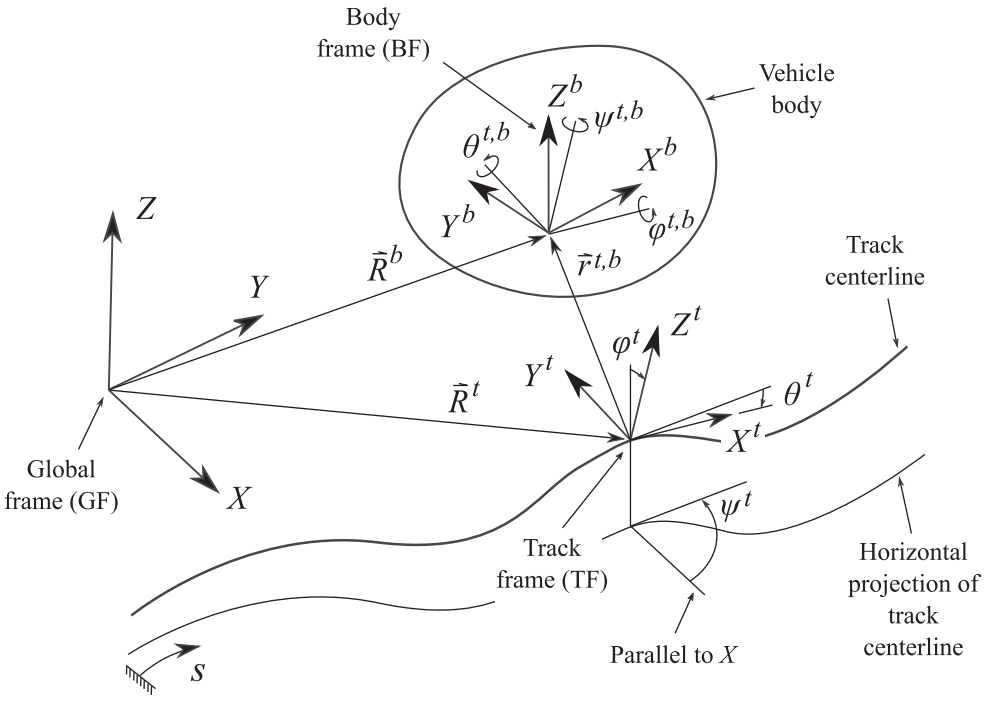

Figure 1. Kinematics of a body with track-relative coordinates.

of an arbitrary point on the design track centreline with respect to the GF is a function of the arc-length s as follows:

$$\mathbf{R}^t(s) = \begin{bmatrix} R_x^t \\ R_y^t \\ R_z^t \end{bmatrix}. \tag{1}$$

And the rotation matrix from the TF to the GF can be approximated to

$$\mathbf{A}^t(s) \simeq \begin{bmatrix} \cos\psi^t & -\sin\psi^t & \varphi^t \sin\psi^t + \theta^t \cos\psi^t \\ \sin\psi^t & \cos\psi^t & \theta^t \sin\psi^t - \varphi^t \cos\psi^t \\ -\theta^t & \varphi^t & 1 \end{bmatrix}, \tag{2}$$

where the Euler angles ψ^t (*azimut* or *heading* angle), θ^t (*vertical slope*) and φ^t (*cant* or *superelevationangle*) that can be observed in Figure 1 have been used. Note that the vertical slope and cant angles are assumed to be small and the rotation matrix is linearised using the small-angle assumption.

The six functions $R_x^t(s)$, $R_y^t(s)$, $R_z^t(s)$, $\psi^t(s)$, $\theta^t(s)$ and $\varphi^t(s)$ are tabulated in the railway industry and they represent the design geometry of the track centreline. In this paper, it is assumed that these functions are given.

Each body b moving along the track has an associated TF at each instant of time. Its position and orientation are obtained substituting the position of the body along the track, $s^b(t)$, in the functions $\mathbf{R}^t(s)$ and $\mathbf{A}^t(s)$.

2.2. Kinematics of a body moving along the track

The coordinates used to describe the position and orientation of the arbitrary body b shown in Figure 1 moving along the track are

$$\mathbf{q}^b = \begin{bmatrix} s^b & r_y^{t,b} & r_z^{t,b} & \varphi^{t,b} & \theta^{t,b} & \psi^{t,b} \end{bmatrix}^{\mathrm{T}}, \tag{3}$$

where s^b is the arc-length along the track of the position of the body, $r_y^{t,b}$ and $r_z^{t,b}$ are the non-zero components of the position vector $\vec{r}^{\,t,b}$ of the BF with respect to the TF, this is $\mathbf{r}^{t,b} = [\ 0 \quad r_y^{t,b} \quad r_z^{t,b}\ ]^{\mathrm{T}}$, and $\varphi^{t,b}$, $\theta^{t,b}$ and $\psi^{t,b}$ are three Euler angles (roll, pitch and yaw, respectively) that define the orientation of the BF with respect to the TF. The arc-length s^b associated with the body can be obtained by finding the plane that, being perpendicular to the track centreline, contains the origin of the BF. The intersection of that plane with the track centreline defines the point where s^b is measured.

The linearised transformation matrix from the BF to the TF is given by

$$\mathbf{A}^{t,b} \simeq \begin{bmatrix} 1 & -\psi^{t,b} & \theta^{t,b} \\ \psi^{t,b} & 1 & -\varphi^{t,b} \\ -\theta^{t,b} & \varphi^{t,b} & 1 \end{bmatrix}. \tag{4}$$

The absolute position vector and the absolute orientation matrix of body b are given by

$$\mathbf{R}^b = \mathbf{R}^t + \mathbf{A}^t \mathbf{r}^{t,b}, \quad \mathbf{A}^b = \mathbf{A}^t \mathbf{A}^{t,b}. \tag{5}$$

The time derivatives of these expressions are used to find the absolute acceleration and angular velocity of body b. See more details in Ref. [19].

2.3. Kinematics of the gyroscope signals

In the remainder of this paper, it will be assumed that an inertial sensor or IMU is installed on the moving body. The IMU is assumed to be installed at the origin of the BF of the moving body with the sensor frame parallel to the BF. The IMU measures the three components of the absolute angular velocity and the three components of the absolute acceleration in the sensor frame. The three signals acquired with the gyroscope are a measure of the absolute angular velocity of the BF as follows:

$$\boldsymbol{\omega}^{imu} = \hat{\boldsymbol{\omega}}^b, \tag{6}$$

where $\boldsymbol{\omega}^{imu}$ is the 3×1 array of the gyroscope signals at a particular instant of time and $\hat{\boldsymbol{\omega}}^b$ contains the three components of the absolute angular velocity in the BF in that time instant. As explained in Ref. [19], the gyroscope signals are related to the absolute Euler angles of body b and their time derivatives as follows:

$$\begin{bmatrix} \hat{\omega}_x \\ \hat{\omega}_y \\ \hat{\omega}_z \end{bmatrix} = \begin{bmatrix} 1 & 0 & -\sin\theta^b \\ 0 & \cos\varphi^b & \sin\varphi^b \cos\theta^b \\ 0 & -\sin\varphi^b & \cos\varphi^b \cos\theta^b \end{bmatrix} \begin{bmatrix} \dot{\varphi}^b \\ \dot{\theta}^b \\ \dot{\psi}^b \end{bmatrix} + \mathbf{u}^{\omega}(t), \tag{7}$$

where $\mathbf{u}^{\omega}(t)$ represents the noise of the gyroscope and $\Phi^b = [\ \varphi^b \quad \theta^b \quad \psi^b\ ]^{\mathrm{T}}$ is the set of absolute angles (with respect to the GF) of the body b. Note that these are not the same

angles given in Equation (3) which are BF to TF relative angles. Using again the small angles assumption of the roll and pitch angles, the following approximation can be adopted:

$$\begin{bmatrix} \hat{\omega}_x \\ \hat{\omega}_y \\ \hat{\omega}_z \end{bmatrix} \approx \begin{bmatrix} \dot{\varphi}^b - \theta^b \dot{\psi}^b \\ \dot{\theta}^b + \varphi^b \dot{\psi}^b \\ \dot{\psi}^b - \varphi^b \dot{\theta}^b \end{bmatrix} + \mathbf{u}^{\omega}(t), \tag{8}$$

which is the set of equations that will be introduced in the Kalman filter as a measurement model for the gyroscope.

Finally, it is useful to specify the relation between the absolute angles $\{\varphi^b, \theta^b, \psi^b\}$ and the track-relative angles $\{\varphi^{t,b}, \theta^{t,b}, \psi^{t,b}\}$:

$$\begin{aligned} \varphi^{t,b} &\approx \varphi^b - \varphi^t, \\ \theta^{t,b} &\approx \theta^b - \theta^t, \\ \psi^{t,b} &\approx \psi^b - \psi^t, \end{aligned} \tag{9}$$

where the assumption that $\{\varphi^{t,b}, \theta^{t,b}, \psi^{t,b}\}$ are small angles has been used.

2.4. Kinematics of the accelerometer signals

Nowadays, most IMU's used in vehicle dynamics have MEMS-type accelerometers. In contrast to piezoelectric accelerometers, the measured signals include the effect of gravity as follows:

$$\mathbf{a}^{imu} = \hat{\ddot{\mathbf{R}}}^b + \left(\mathbf{A}^b\right)^{\mathrm{T}} \begin{bmatrix} 0 & 0 & g \end{bmatrix}^{\mathrm{T}} + \mathbf{u}^{ac}(t), \tag{10}$$

where $\mathbf{a}^{imu}$ is the 3×1 array of the accelerometer signals, $\hat{\ddot{\mathbf{R}}}^b$ contains the three components of the absolute acceleration of the IMU in the sensor frame, $\mathbf{A}^b$ is the absolute rotation matrix of the IMU, $\mathbf{u}^{ac}(t)$ represents the accelerometer noise and g is the acceleration of gravity that is assumed to act in the Z direction. Equation (10) can also be written as

$$\mathbf{a}^{imu} = \left(\mathbf{A}^{t,b}\right)^{\mathrm{T}} \bar{\ddot{\mathbf{R}}}^b + \left(\mathbf{A}^b\right)^{\mathrm{T}} \begin{bmatrix} 0 & 0 & g \end{bmatrix}^{\mathrm{T}} + \mathbf{u}^{ac}(t), \tag{11}$$

where $\bar{\ddot{\mathbf{R}}}^b$ represents the absolute acceleration of the IMU projected onto the TF. It is shown in Ref. [19] that vector $\bar{\ddot{\mathbf{R}}}^b$ can be developed as

$$\begin{aligned} \bar{\ddot{\mathbf{R}}}^b = &\begin{bmatrix} \dot{V} \\ \rho_h V^2 \\ -\rho_v V^2 \end{bmatrix} + \begin{bmatrix} 0 \\ \ddot{r}_y^{t,b} \\ \ddot{r}_z^{t,b} \end{bmatrix} \\ &+ \begin{bmatrix} -r_y^{t,b}\left(\dot{V}\rho_h + V^2(\rho_h' - \rho_{tw}\rho_v)\right) + r_z^{t,b}(V^2\rho_{tw}\rho_v + \dot{V}\rho_v) \\ -r_y^{t,b}\left(V^2(\rho_{tw}^2 + \rho_h^2)\right) + r_z^{t,b}(V^2\rho_v\rho_h - \dot{V}\rho_{tw}) \\ r_y^{t,b}(V^2\rho_v\rho_h + \dot{V}\rho_{tw}) - r_z^{t,b}\left(V^2(\rho_{tw}^2 + \rho_v^2)\right) \end{bmatrix} \\ &+ 2\begin{bmatrix} V\rho_v\dot{r}_z^{t,b} - V\rho_h\dot{r}_y^{t,b} \\ -V\rho_{tw}\dot{r}_z^{t,b} \\ V\rho_{tw}\dot{r}_y^{t,b} \end{bmatrix}, \end{aligned} \tag{12}$$

where V is the forward velocity of the body and ρ_h, ρ_v and ρ_{tw} are the horizontal, vertical and twist curvatures, respectively, of the track centreline. The prime represents differentiation with respect to s.

Introducing Equations (2), (4), (5) and (12) into Equation (11) provides vector $\mathbf{a}^{imu}$ as the sum of the noise term $\mathbf{u}^{ac}(t)$ and a nonlinear function of the position and orientation of body b and their time derivatives. This expression, which is not presented here because of its considerable length, can be found in Appendix 1.

Finally, note that the second term in the r.h.s. of Equation (11) can be used to obtain the direction of gravity (vertical) with respect to the sensor frame. These values are used in inclinometers to measure the orientation of a body. In that sense, it can be said that our method does use an inclinometer. In other words, our accelerometer is used to measure the acceleration and, in part, the orientation of the sensor frame, as done in an inclinometer.

3. Kalman filter

A Kalman filter approach is proposed to obtain the trajectory and attitude of the moving body from the IMU measurements. Please note that the term *Kalman filter* is used in a broad sense throughout the paper, since the procedure applied to obtain the position and orientation of the moving body is actually a *first-order extended Kalman smoother* [31].

For the Kalman filter that we use in this research, a purely kinematic process model has been chosen. Alternatively, a dynamic model based on the equations of motion of a rail vehicle moving along the track could be used as the process model. The kinematic model is preferable because it requires less parameters to identify, being all of them geometric (easy to find). Besides, the kinematic model is valid for all bodies of the vehicle. Dynamic models need many more parameters that are more difficult to identify (position of centres of gravity, inertia tensors, stiffness constants, viscous-equivalent damping constants, etc.) and vary depending on the selected body of the vehicle.

Before defining the Kalman filter, it is useful to clarify the chosen nomenclature for the *state space model*:

$$\left\{\begin{array}{l} \boldsymbol{x}_{k+1} = \mathbf{F}\boldsymbol{x}_k + \boldsymbol{q}_k \\ \boldsymbol{z}_k = \mathbf{g}(\boldsymbol{x}_k) + \boldsymbol{u}_k \end{array}\right\} \quad \text{with} \quad \left\{\begin{array}{l} \boldsymbol{q}_k \sim \mathbf{N}(\mathbf{0}, \mathbf{Q}) \\ \boldsymbol{u}_k \sim \mathbf{N}(\mathbf{0}, \mathbf{U}) \end{array}\right\}. \tag{13}$$

- $\boldsymbol{x}_k$: state vector of the system at time instant k.
- $\boldsymbol{z}_k$: measurements vector at time instant k.
- $\mathbf{F}$: transition matrix of the system.
- $\mathbf{g}(\boldsymbol{x}_k)$: measurement model given as a nonlinear function of the state.
- $\mathbf{Q}$: Process noise covariance matrix.
- $\mathbf{U}$: Measurements noise covariance matrix.
- $\mathbf{N}(\mathbf{M}, \mathbf{S})$: Multivariate normal random variable with mean $\mathbf{M}$ and covariance matrix $\mathbf{S}$.

The proposed Kalman filter simultaneously estimates the absolute orientation of the moving body and its position relative to the track, given by variables $\{\varphi^b, \theta^b, \psi^b, r_y^{t,b}, r_z^{t,b}\}$. The algorithm exploits the kinematic model given by Equations (8), (9) and (11).

In order to avoid the drift of the position variables $\{r_y^{t,b}, r_z^{t,b}\}$, it is convenient to include the following additional equation in the Kalman filter:

$$\begin{bmatrix} r_y^{t,b} \\ r_z^{t,b} \end{bmatrix} = \begin{bmatrix} 0 \\ \delta \end{bmatrix} + \mathbf{u}^{pos}(t), \tag{14}$$

which constitutes a pair of fictitious position measurements with noise $\mathbf{u}^{pos}(t)$ [32]. Parameter δ represents the vertical distance at rest between the IMU and the track design centreline.

The state vector is defined as

$$\boldsymbol{x} = \begin{bmatrix} \varphi^b & \dot{\varphi}^b & \theta^b & \dot{\theta}^b & \psi^b & \dot{\psi}^b & r_y^{t,b} & \dot{r}_y^{t,b} & \ddot{r}_y^{t,b} & r_z^{t,b} & \dot{r}_z^{t,b} & \ddot{r}_z^{t,b} \end{bmatrix}^{\mathrm{T}}. \tag{15}$$

Note that the arc-length coordinate s^b and its time derivatives are not included in $\boldsymbol{x}$. The reason is that this coordinate is estimated using an independent odometry algorithm described in Ref. [19]. This algorithm is very accurate for practical purposes but not as accurate as to detect longitudinal vibrations in the vehicle. Therefore, the Kalman filter cannot detect the influence on the body trajectory of the longitudinal vibrations of the vehicle.

Using Equations (8), (9), (11), (14) and (15), all vectors and matrices required to formulate the state space model (13) can be obtained. These are presented in Appendix 1 for better clarity. In the next paragraphs, the proposed model and the assumptions on which it is based are discussed.

Regarding the process model, a purely kinematic representation of the system has been chosen, for reasons that have already been outlined at the beginning of this section. It is worth examining with some detail the consequences of this kind of modelling. Consider, for example, the relation between successive accelerations in y direction (the reasoning is analogous for the z direction), which takes the form $\ddot{r}_{y,k+1}^{t,b} = \ddot{r}_{y,k}^{t,b} + f_k$. It is clear that the term f_k will depend on the variation, between instants k and $k+1$, of the forces acting on body b. If b is the car body of the vehicle, these forces will be mainly transmitted through the suspension system. However, taking a purely kinematic approach means that we decide not to model the forces acting upon the system, which frees us from having to define stiffness constants, masses, moments of inertia, etc. The consequence is that the term f_k remains unknown and can only be modelled as a random variable. In the presented approach, as is shown in Appendix 1, the term f_k has been modelled as a Gaussian random variable with zero mean and a variance proportional to the sampling interval. This corresponds to the assumption that the acceleration follows a Wiener process between instants k and $k+1$, which is a rather usual kinematic model [31,33], sometimes referred to as *Wiener process acceleration state model* in the literature. It could be argued that the hypothesis that accelerations evolve between measurements as Wiener processes is not actually met by a railway vehicle, which is a reasonable objection. It is true that such a process model by itself could not provide anything like the real vehicle motion. However, it will be shown that, when this type of process model is put together with the appropriate measurement model, the results can be reasonably accurate, even if the statistical assumptions for the construction of the process equations are not rigorously met.

The proposed process model also includes the assumption that angular velocities evolve as Wiener processes between measurements, analogously to the described model for linear

accelerations. These hypotheses provide a covariance matrix $\mathbf{Q}$ with the form presented in Appendix 1.

Regarding the measurement equations, we assume each measurement to have a Gaussian noise with zero mean and no correlation between samples, characterised by a covariance matrix $\mathbf{U}$. This is a reasonable assumption for the IMU measurements, although there could be some noise colouration if the sampling interval was too small. On the other hand, it is interesting to note the implications of this kind of modelling with respect to the virtual position measurements (Equation (14)). Focusing on the position in y direction (the situation is analogous for the position in z direction), it is assumed that, at each instant k, position $r_y^{t,b}$ is a random Gaussian variable with zero mean and certain variance, without any dependence on previous instants. Of course, this assumption does not represent the true dynamics of the vehicle motion. Nevertheless, in the absence of any real position sensor, a virtual measurement such as given in Equation (14) is an effective means to avoid the drift of the position variables (see the work from Naets et al. [32] for a thorough justification of this technique). As was mentioned with regards to the process model, it will be shown that the Kalman filter can provide sufficiently accurate estimations even when some of the statistical model assumptions are not met by the real system.

It can be observed in Appendix 1 that 13 parameters are required to fully define covariance matrices $\mathbf{Q}$ and $\mathbf{U}$. These parameters are gathered in a vector $\mathbf{p}$:

$$\mathbf{p} = \begin{bmatrix} q_\varphi & q_\theta & q_\psi & q_y & q_z & u_x^\omega & u_y^\omega & u_z^\omega & u_x^{ac} & u_y^{ac} & u_z^{ac} & u_y^{pos} & u_z^{pos} \end{bmatrix}^{\mathrm{T}}. \quad (16)$$

The meaning of each of these parameters is specified below:

- $\{q_\varphi, q_\theta, q_\psi\}$: power spectral density (PSD) of the roll, pitch and yaw angular accelerations, respectively.
- $\{q_y, q_z\}$: PSD of the jerk (time derivative of the linear acceleration) in y and z directions, respectively.
- $\{u_x^\omega, u_y^\omega, u_z^\omega\}$: variance of the gyrometer noise in its three directions.
- $\{u_x^{ac}, u_y^{ac}, u_z^{ac}\}$: variance of the accelerometer noise in its three directions.
- $\{u_y^{pos}, u_z^{pos}\}$: variance of the noise associated with the fictitious position measurements in y and z directions, respectively.

4. Methods for the estimation of covariance matrices

In the last section, a Kalman filtering approach has been presented with the aim of estimating the trajectory and attitude of a rigid body b moving along a railway track. To be able to use this algorithm, the first step is to fully define covariance matrices $\mathbf{Q}$ and $\mathbf{U}$ in Equation (13).

We use $\mathbf{p} = \begin{bmatrix} p_1 & p_2 & \cdots & p_M \end{bmatrix}^{\mathrm{T}}$ to denote a vector containing the scalar parameters that determine matrices $\mathbf{Q}$ and $\mathbf{U}$. The number of elements in $\mathbf{p}$ is $M = 13$ for the Kalman filter under consideration (see Equation (16)).

Before proceeding to describe the proposed strategies to estimate vector $\mathbf{p}$, some clarifications are appropriate. The developments presented in Sections 2 and 3 are completely general, in the sense that they can be used in any application that requires estimating the position and orientation of a vehicle moving along a railway track. On the other hand,

these techniques have been applied in the current research to the specific problem of measuring track irregularities. A *track geometry measuring system* (TGMS) has been developed by the authors, combining computer vision with the estimation of the trajectory and attitude of the vehicle using inertial sensors (see Ref. [19] for details). The present section expounds two alternative procedures to estimate vector **p**. The first one is specific to the TGMS application, while the second one is as general as Sections 2 and 3:

- Known-output method (KOM). The covariance matrices are tuned through a comparison between the track irregularities obtained experimentally with the TGMS and a set of *reference irregularities*.
- Constrained maximum likelihood (CML) estimation. This technique uses the IMU measurements to obtain the *most likely* vector **p**.

In both cases, a global optimisation of certain objective function is conducted, with the components of vector **p** varying within a specified range. In order to choose appropriate range limits, consider first that every parameter p_i must be positive due to their physical meaning – see Section 3. On the other hand, the range should be wide enough to encompass a meaningful optimum of the objective function. After several trials, the following range has been found to produce accurate results:

$$10^{-4} \leq p_i \leq 10^4 \text{ for } \quad i = 1, \ldots, M \tag{17}$$

with each p_i measured in SI.

After testing different global optimisation techniques included in the *MATLAB optimisation toolbox*, the method that was found to work best for this application was the *surrogate optimisation* [34].

4.1. KOM

In order to apply the KOM, the vehicle with the operating TGMS has to travel along a track whose irregularities have already been obtained through some other reliable methodology (reference irregularities). For the present work, these reference irregularities were obtained using an LVDT, an inclinometer and a total station, as described in detail in Ref. [35].

It is convenient at this point to recall that we are interested in the four irregularities that are usually controlled in the railway industry:

- Absolute irregularities: alignment (ξ_{al}) and vertical profile (ξ_{vp}).
- Relative irregularities: gauge variation (ξ_{gv}) and cross-level (ξ_{cl}).

'Absolute' and 'relative' mean that the first two irregularities are those of the track centreline while the last two are relative irregularities of the left rail with respect to the right rail. See Ref. [19] for precise definitions of these terms.

The optimisation algorithm searches for the vector **p** that minimises the root mean square (RMS) of the difference between the TGMS irregularities and the reference irregularities. Thus, the objective function for the optimisation, f, is defined as

$$f = (\xi_{al}^{tgms} - \xi_{al}^{ref})_{\text{RMS}} + (\xi_{vp}^{tgms} - \xi_{vp}^{ref})_{\text{RMS}} + (\xi_{cl}^{tgms} - \xi_{cl}^{ref})_{\text{RMS}}, \tag{18}$$

where reference irregularities are labelled with superscript *ref* and irregularities obtained with the TGMS are labelled with superscript *tgms*.

Note that the gauge variation is not included in (18). The reason is that this irregularity has been found to depend almost exclusively on the computer vision system of the TGMS, with a negligible influence of the vehicle trajectory and attitude.

Let us make some remarks about the described strategy:

- From a pragmatic point of view, this approach has a clear disadvantage: when installing the TGMS on a new commercial vehicle, it would need to travel along a track whose irregularities were reliably known beforehand, which is not easy to find in practice. Furthermore, the appeal of the TGMS technology could get limited by the need of a complex initial calibration.
- This procedure relies on the assumption that once the covariance matrices have been estimated for a certain track, with certain levels of irregularity and a vehicle circulating at certain speed, the Kalman filter will still produce accurate results for other tracks, with different irregularities and different vehicle speeds. The validity of this hypothesis is not evident. Fortunately, the CML estimation procedure is not subjected to this potential drawback, as discussed in the next subsection.

4.2. CML estimation

Constrained maximum likelihood estimation (MLE) is a very common approach for tuning the parameters of statistical models — the meaning of the word *constrained* in the title of this subsection will be seen at the end of it. The basic idea is the following. Consider a generic multivariate random variable $\mathbf{y}$ whose probability density function, $p(\mathbf{y}|\mathbf{p})$, depends on a set of parameters $\mathbf{p}$. Given a specific observation $\mathbf{y}_0$, we estimate $\mathbf{p}$ as the set of parameters that maximises $p(\mathbf{y}_0|\mathbf{p})$. That is to say, we choose the parameters that are most likely to generate the observed data. For a more complete explanation of the MLE concept, see Ref. [36].

The generic scheme outlined above can be directly particularised to the trajectory and attitude estimation that is being investigated. While the vector of parameters $\mathbf{p}$ is given in Equation (16), the set of observed data $\mathbf{y}_0$ represents the sequence of accelerations, angular velocities, forward speeds and positions along the track registered during a specific ride of the moving body b (Figure 1). Finally, the probability density of the observations $p(\mathbf{y}|\mathbf{p})$ can be obtained from the model equations (13), as shown in Ref. [37].

In summary, given a set of observations $\mathbf{y}_0$, the proposed global optimisation algorithm will explore the space of parameters $\mathbf{p}$ within the range specified in Equation (17), searching for those parameter values that maximise $p(\mathbf{y}_0|\mathbf{p})$. The specific equations that need to be appended to the Kalman filter algorithm in order to calculate $p(\mathbf{y}_0|\mathbf{p})$ can be found in Ref. [37].

Note that, when the described methodology is used for the TGMS application, it has a plain advantage over the one set forth in Section 4.1, since in this case there is no need for a previously known set of irregularities to tune the covariance matrices. Consider further the following benefit: assume that a railway vehicle, with an operating TGMS, performs two rides on two very different tracks, with different irregularity levels and moving at different forward speeds. As was commented in Section 4.1, it is not obvious that only one pair of

matrices **Q** and **U** could provide accurate results for both tracks. The MLE would take this automatically into account by obtaining one set of *most likely* covariance matrices for each of the rides. Of course, this can also be said about different portions of the same vehicle ride. It might be appropriate, for example, to use different **Q** matrices for curves and for straight portions of the track. This kind of differentiation can easily be implemented when using CML estimation, as discussed in more detail in Section 6.1.

4.2.1. Constraints imposed for the optimisation

The experimental results obtained during this research have shown that the MLE, as has been described, can produce inaccurate outcomes in this application. That is to say, the most likely covariance matrices do not necessarily provide a good position and attitude estimation. This problem has been solved by slightly guiding the search for the optimum with the following constraint on the parameters:

$$u_y^{ac} \leq u_y^{pos}/10 \tag{19}$$

with both parameters measured in SI.

From the physical meaning of u_y^{ac} and u_y^{pos}, specified at the end of Section 3, Equation (19) can be interpreted as follows: *measuring all parameters in SI, the Kalman filter must have a considerably higher confidence in the accelerometer measurements in y direction than it has in the virtual position measurements in y direction*. This way, we avoid the optimisation process from leading to a solution of the type $r_y^{t,b}(t) \approx 0$ due to an excessive weight of the fictitious position measurements in the calculations.

It can be said after the above considerations that, instead of a plain MLE, the proposed approach falls within the category of *CML estimation* [38,39].

5. TGMS method and experimental setup

The TGMS is a technology developed by the authors for the measurement of the irregularities of rail tracks. It combines inertial sensors with computer vision, as schematically represented in Figure 2. This technology is explained in detail in Ref. [19].

Results shown in Ref. [19] are obtained with a 1:10 scale experimental facility installed at the School of Engineering of the University of Seville. Figure 3 shows the 90 m-scale track that has been designed to create an arbitrary distribution of irregularities, while Figure 4 displays the scale vehicle used in the experiments, which incorporates the TGMS. In this case, body b, whose trajectory and orientation will be estimated, is the vehicle carbody. It is important to emphasise that the TGMS allows the installation of the sensors on any body of the vehicle. The track includes a 22 m straight section and two curved sections of 26 m and 12 m, among other features.

Note that algorithms for the estimation of the trajectory and attitude of the IMU were already used in the TGMS presented in Ref. [19]. The methods developed in this paper improve the Kalman filter model and the estimation of the covariance matrices compared with the equivalent methods given in Ref. [19]. As a consequence, the estimation of the track irregularities is substantially improved also, as will be shown in Section 6.

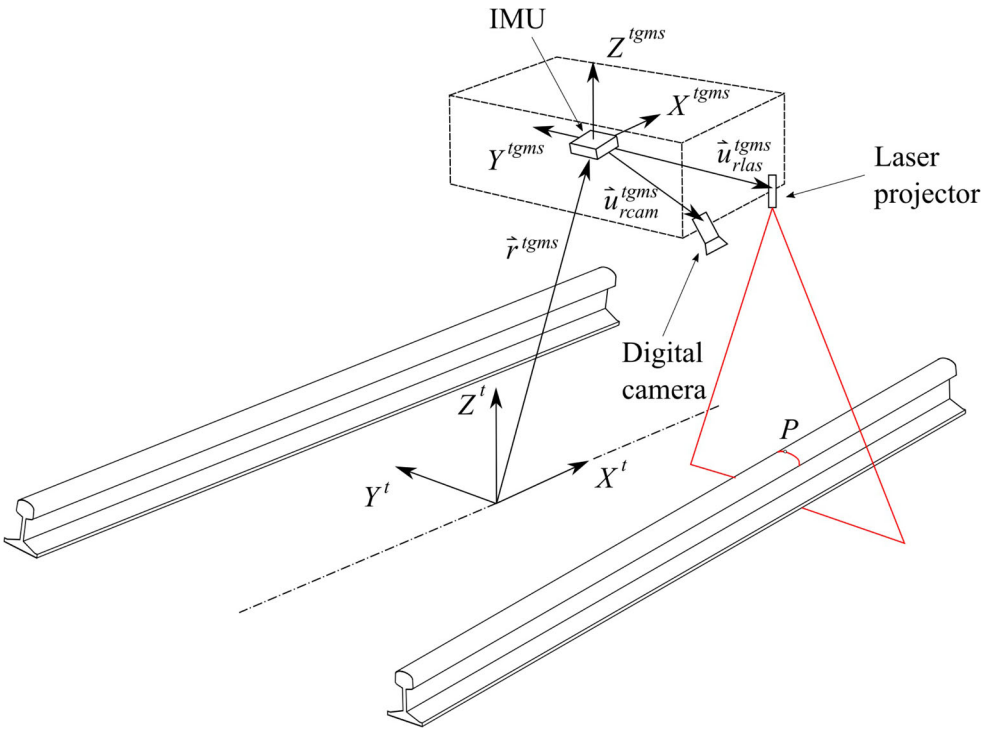

Figure 2. TGMS.

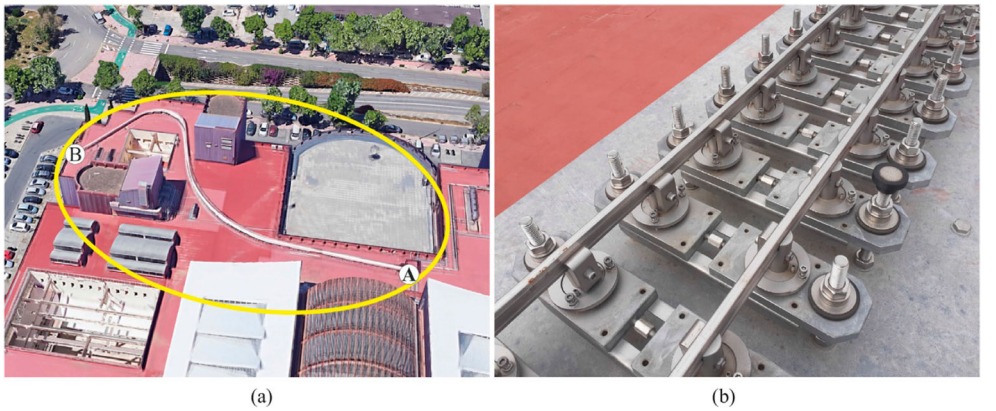

Figure 3. Scale track: (a) aerial view and (b) detail of track supports.

6. Results

This section presents the experimental results that have been obtained when applying the procedures developed in this paper to the problem of track geometry measurement, as described in Section 5. For the details on how the trajectory and attitude estimation is used within the TGMS technology to measure track irregularities, see Ref. [19]. This technology can be used to obtain gauge, cross-level, alignment and vertical profile. However,

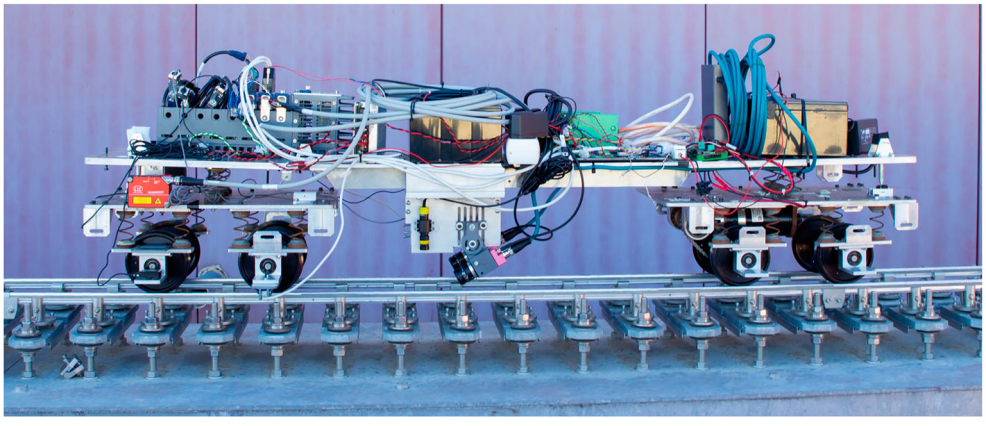

Figure 4. Scale vehicle with TGMS.

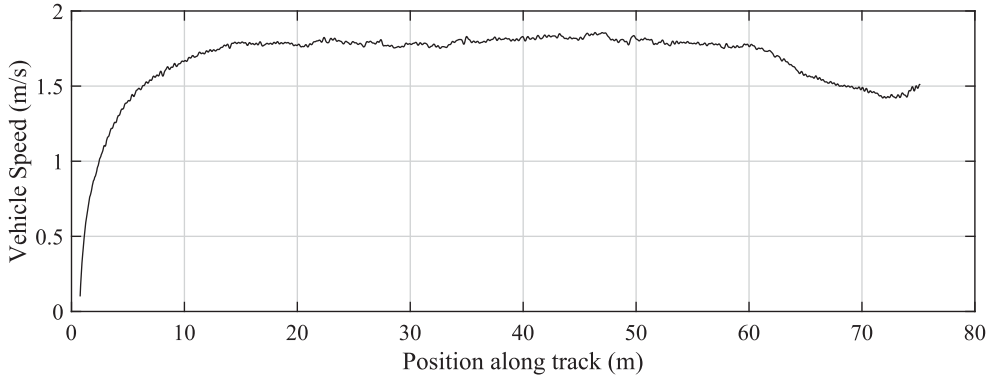

Figure 5. Forward velocity of the scale vehicle during the test.

the influence of the position and orientation of the TGMS in the measurement of the gauge is very little (video cameras provide almost all the data that are needed). For this reason, the gauge is excluded from the results presented next.

The reference geometry of the scale track was measured using a LVDT sensor for the gauge, an inclinometer for the cross-level and a high-accurate robotic total station for the alignment and vertical profile. The procedure is described in Ref. [35]. Results are labelled as 'Reference' in the plots shown in Appendix 2. These reference results can be considered as equivalent to the ones that can be obtained with a RTT with total station, which is the most accurate device used in the industry to measure track irregularities. Reference irregularities are measured in the unloaded track. Measurements taken from the scale vehicle with TGMS measure the loaded track irregularities. In the case of the scale track, deformation due to the vehicle action is not significant. However, in real scale tracks, if the geometry measurements are made from a heavy vehicle, the unloaded and loaded track irregularities may differ significantly. Reference irregularities are compared with the estimations obtained using the measurements taken during one ride of the instrumented vehicle along the scale track with the forward velocity shown in Figure 5.

Table 1. Quantitative evaluation of the difference between the cross-level provided by the TGMS and the reference cross-level: μ (mean value), σ (standard deviation) and Max (maximum absolute value).

	Cross-level (unfiltered)			Cross-level (filtered)		
	μ (mm)	σ (mm)	Max (mm)	μ (mm)	σ (mm)	Max (mm)
CML estimation	0.054	0.162	1.185	0.004	0.119	1.051
KOM	0.028	0.167	1.242	0.002	0.114	1.105
KOM for 0.8 m $< s <$ 45 m	0.032	0.173	1.280	0.002	0.111	1.053
KOM for 45 m $< s <$ 65 m	−0.063	0.500	2.509	0.0004	0.119	1.211
CML estimation with added noise	0.053	0.166	1.161	0.003	0.119	1.050

Some of the irregularity profiles displayed throughout this section are filtered. Whether or not each particular irregularity has been filtered for the representation is specified in the corresponding figure caption (Figures A1–A2). Filtered irregularities only preserve wavelengths between 0.3 m and 7 m. European Standard [40] states that irregularity wavelengths between 3 m and 70 m are the ones directly associated with railway vehicles safety. These wavelengths are divided by the scale factor to find the cut-off wavelengths of the applied filter.

The rest of this section is divided into three subsections. Section 6.1 compares the reference irregularities with those obtained using the TGMS, both applying CML estimation and KOM for the covariance matrices. In Section 6.2, we analyse the confidence intervals for the irregularities obtained using CML estimation. Finally, Section (6.3) evaluates the results provided by the TGMS using CML estimation when artificial noise is added to the IMU signals. This is intended to assess the sensitivity of the algorithm to a drop in sensor quality. The graphical representation of all the obtained results is shown in Appendix 2.

6.1. Performance of CML estimation and KOM

The results presented in Figure A1 show that the irregularity profiles provided by the TGMS are remarkably accurate, either using CML estimation (except for a spurious alignment peak at the beginning of the test) or KOM to obtain the covariance matrices. This is evidenced by the similarity between the reference irregularities and those yielded by the TGMS. The achieved accuracy is quantified in Tables 1 and 2. Although a standard deviation of more than 1 mm for the alignment in Table 2 might seem excessive, it should be noted that this value is highly affected by the mentioned initial spurious peak. If this initial portion of the track is disregarded, the standard deviation falls to 0.7 mm, which is more acceptable. The reason for the clear alignment inaccuracy during the first metres of the ride will require further investigation in the future.

It should be mentioned that the results presented in Figure A1 were obtained for constant covariance matrices $\mathbf{Q}$ and $\mathbf{U}$. However, as was discussed in Section 4.2, one of the main advantages of CML estimation is that it allows for the estimation of different covariance matrices for different portions of the track. This was done for the test under consideration, dividing the track into its straight and curved segments. Since, in this case, no improvement was found with respect to the calculation with constant $\mathbf{Q}$ and $\mathbf{U}$, the results corresponding to varying covariance matrices are not shown in the paper. In any case, the fact that this differentiation between portions of the track is easily implementable with CML estimation constitutes a highly advantageous feature — in general, better results

Table 2. Quantitative evaluation of the difference between the absolute irregularities provided by the TGMS and the absolute irregularities of reference: μ (mean value), σ (standard deviation) and Max (maximum absolute value).

	Alignment (filtered)			Vertical profile (filtered)		
	μ (mm)	σ (mm)	Max (mm)	μ (mm)	σ (mm)	Max (mm)
CML estimation	0.040	1.030	6.952	0.008	0.375	1.877
KOM	−0.017	0.659	3.621	0.005	0.360	1.800
KOM for 0.8 m $< s <$ 45 m	−0.005	0.891	3.369	0.007	0.356	1.828
KOM for 45 m $< s <$ 65 m	−0.007	0.792	3.471	0.007	0.356	1.844
CML estimation with added noise	0.024	0.999	5.641	0.007	0.368	1.869

can be expected if the covariances are optimised for each specific condition of the vehicle motion.

Since both KOM and CML estimation provide reasonably accurate results, and taking into account the benefits and weaknesses discussed in Section 4 for both methods, CML estimation seems to be the most promising algorithm for the TGMS. For this reason, the two remaining subsections focus on the results obtained with CML estimation.

6.2. Confidence intervals obtained with CML estimation

A relevant and often overlooked feature of the Kalman filter algorithm is that, together with the sequence of expected system states, it also provides the sequence of covariance matrices for the system state. This means that we have a quantification of the level of uncertainty associated with the Kalman filter estimation, which allows for the computation of confidence intervals.

The 95% confidence intervals for the irregularities obtained with CML estimation are shown in Figure A3, together with the reference irregularities. In principle, the proportion of the complete track for which each reference irregularity falls within the confidence interval should be around 95%. However, the percentages obtained from Figure A3 turn out to be considerably different: 49% for the unfiltered cross-level, 73% for the filtered cross-level, 98% for the filtered alignment and 99% for the filtered vertical profile. The confidence interval seems to be too narrow for the cross level and too wide for the alignment and vertical profile. Possible reasons for this discrepancy are discussed in the next paragraphs.

First, it is clear that the irregularities obtained using the TGMS have additional sources of uncertainty other than those associated with the trajectory and attitude estimation. For example, the uncertainty of the artificial vision system of the TGMS is not included in the construction of the confidence intervals presented in Figure A3, which may distort the results.

On the other hand, it is highly probable that the mismatch of the confidence intervals is also due to the statistical assumptions of the state space model. As was discussed in Section 3, some of the hypotheses on which the model is built are not met by the real system, namely the assumption that linear accelerations and angular velocities evolve as Wiener processes between samples (process model) and the assumption that the positions in y and z direction are, at each considered instant, Gaussian random variables with no dependence between samples (virtual position measurements, Equation (14)). It is convenient to recall that these two assumptions have been introduced as a means to eliminate

the need for position sensors and for a dynamic model of the system. The rationale is clear: if, even with the mentioned assumptions, the algorithm was found to provide sufficiently accurate results, this would constitute a relevant step towards making the estimation of trajectory and attitude of railway vehicles as simple and practical as possible.

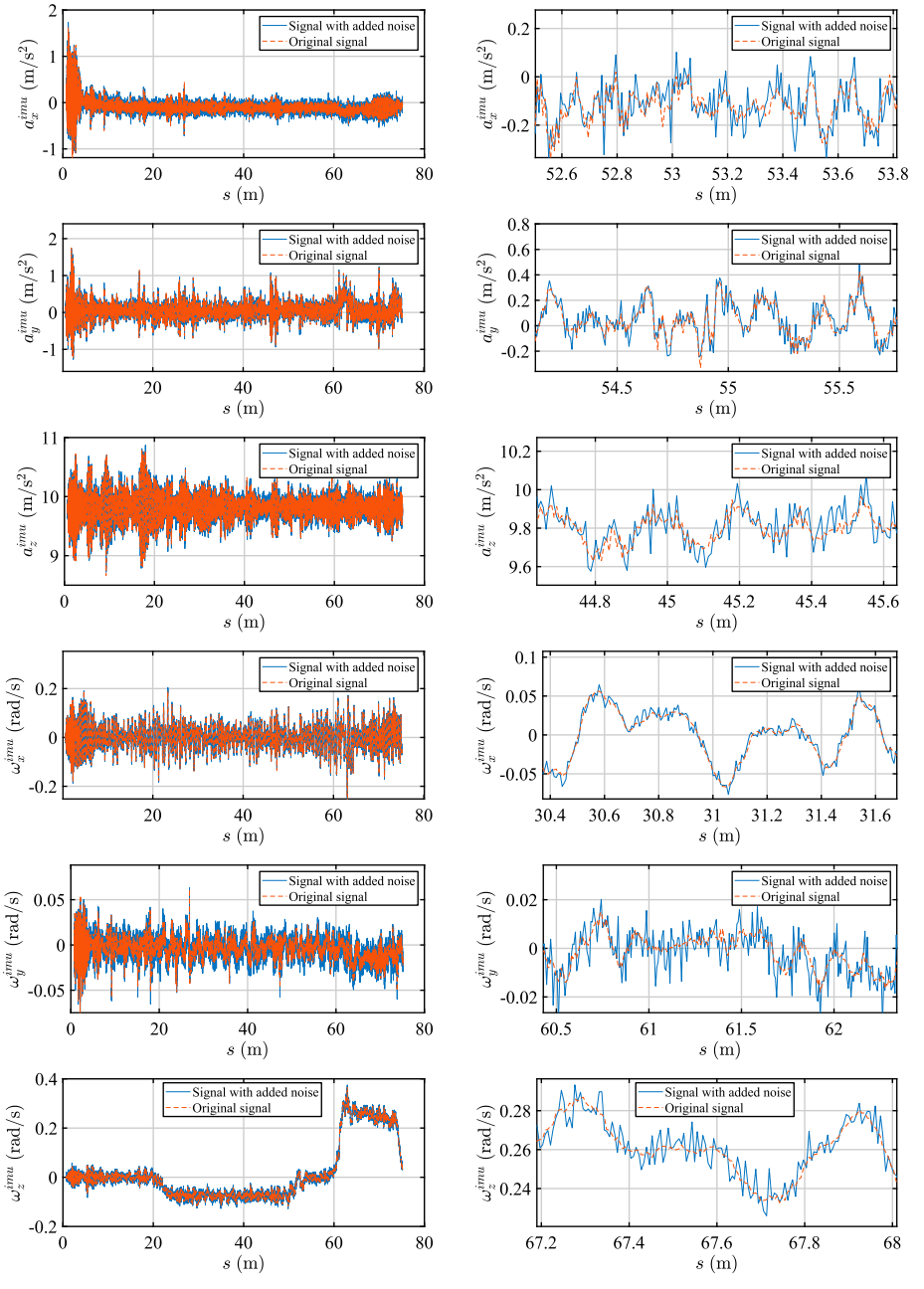

Figure 6. IMU signals with and without added noise. Each graph on the right is a close-up view of the corresponding graph on the left.

The results presented in Figure A1 show that the Kalman filter with CML estimation provides the trajectory and orientation of the vehicle with notable accuracy. However, Figure A3 indicates that the obtained confidence intervals are not reliable. In other words, the proposed algorithm is able to produce accurate estimates for the system state (trajectory and orientation of the vehicle) but does not correctly quantify the uncertainty of this estimation. This was actually expectable, considering the assumptions made. In fact, the same kind of result can be found with a simple synthetic example where certain periodic displacement in one dimension is tracked using a noisy acceleration *measurement* (true known acceleration + artificial noise) and a fictitious position measurement such as given in Equation (14), together with a process model that assumes the acceleration to evolve as a Wiener process between samples: the Kalman filter is able to accurately estimate the sequence of positions, but not its confidence intervals. Note that even without a good estimation of the uncertainty, having a reliable estimate of the trajectory and attitude of a railway vehicle can be highly useful for practical purposes.

6.3. Performance of CML estimation with added IMU noise

This subsection intends to evaluate the sensitivity of the proposed algorithm to the quality of the IMU. For this assessment, some artificial Gaussian noise has been added to each of the IMU signals, as represented in Figure 6. The estimated irregularities, with and without this additional noise in the inertial measurements, are represented in Figure A2, together with the reference irregularities. It can be observed that the irregularity estimation remains reasonably accurate despite the extra noise, which suggests that the proposed methodology can provide good results even with an IMU of moderate quality and cost.

7. Summary and conclusions

This paper addresses the estimation of the trajectory and attitude of a body moving along a railroad track. Compared with the equivalent, and well developed in the literature, estimation problems used for inertial navigation of air or road vehicles, this problem has two specific properties: (1) the resulting trajectory and attitude are very similar to the known trajectory and attitude of the track centreline and (2) the required accuracy is very demanding for applications like track geometry measurement. The developed estimation techniques are based on the kinematics of an arbitrary body moving along an arbitrary track and the exact relationship between the description of this type of motion and the measurements of inertial sensors.

The estimations are based on the discrete first-order extended Kalman smoother (simply *Kalman filter* for short). This procedure requires assigning appropriate values to the parameters of the process noise and measurement noise covariance matrices. Two methods are used in this work to calculate these parameters: the KOM and the CML estimation. The KOM, which is specific for the application of track geometry measurement, requires the use of a railroad track with known irregular geometry. The CML estimation is much more general and does not rely upon the previous knowledge of any irregularity profiles. Both techniques are explained in detail. In this paper, the Kalman filter and the methods for the estimation of the covariance matrices are used as described in the scientific literature. No contributions are done to these methods.

The proposed approach is experimentally validated using a 1:10 scale track. Results show a remarkably accurate estimation of the track irregularities, using either the KOM or CML estimation for the covariance matrices. Therefore, it is obvious to propose the use of the much simpler and less costly CML estimation procedure, which also has the advantage of being able to provide different covariance matrices for each specific condition of the vehicle motion. It should be mentioned that although the proposed CML estimation yields accurate irregularity profiles, it does not provide reliable confidence intervals, probably due to the statistical assumptions of the model. In any case, thanks to the applied estimation techniques, the precision of the measurement of the track irregularities has improved significantly with respect to the results presented in Ref. [19]. In addition, the CML estimation is found to be considerably robust against IMU noise.

Finally, it should be stressed that the method presented in this paper to measure the trajectory and attitude of a body moving along a rail track can be used with the same level of accuracy regardless of the length of the track. To this end, an odometry algorithm for the estimation of the body position along the track that does not suffer of signal drift must be used, as the one described in Ref. [19]. This is a key aspect that allows this method to be used to measure the track geometry without the need of total station or GNSS.

Acknowledgments

The authors would like to sincerely thank Prof. Javier Ros, from the Public University of Navarra, for his useful comments and technical suggestions on the applied Kalman filtering techniques.

Disclosure statement

No potential conflict of interest was reported by the authors.

Funding

This research was supported by the Spanish Ministerio de Ciencia e Innovación, under the programme 'Proyectos I+D+I–2020', with project reference PID2020-117614RB-I00. This support is gratefully acknowledged.

Data availability

The datasets generated and analysed during the current study are available from the corresponding author on reasonable request.

References

[1] Ahmad I, El Hadri A, Benziane L, et al. Globally asymptotic attitude estimation for accelerated aerial vehicles. Aerosp Sci Technol. 2019;84:1175–1181. doi:10.1016/j.ast.2018.06.008
[2] Bryne TH, Rogne RH, Fossen TI, et al. Attitude and heave estimation for ships using MEMS-based inertial measurements. IFAC-PapersOnLine. 2016;49(23):568–575. doi:10.1016/j.ifacol.2016.10.496
[3] Hua MD. Attitude estimation for accelerated vehicles using GPS/INS measurements. Control Eng Pract. 2010;18(7):723–732. doi:10.1016/j.conengprac.2010.01.016

[4] Scholte WJ, Rodrigo Marco V, Nijmeijer H. Experimental validation of vehicle velocity, attitude and IMU bias estimation. IFAC-PapersOnLine. 2019;52(8):118–123. doi:10.1016/j.ifacol.2019.08.058
[5] Aldimirov M, Arnaudov R. Method for automated reconstruction of a car's path during crash from GPS/INS data using a Kalman filter. Adv Eng Softw. 2018;115:386–390. doi:10.1016/j.advengsoft.2017.10.009
[6] Vaganay J, Aldon MJ. Attitude estimation for a vehicle using inertial sensors. Control Eng Pract. 1994;2(2):281–287. doi:10.1016/0967-0661(94)90209-7
[7] Anderle M, Čelikovský S. Sensor fusion for simple walking robot using low-level implementation of extended Kalman filter. IFAC-PapersOnLine. 2018;51(13):43–48. doi:10.1016/j.ifacol.2018.07.252
[8] Kada B, Munawar K, Shaikh MS, et al. UAV attitude estimation using nonlinear filtering and low-cost mems sensors. IFAC-PapersOnLine. 2016;49(21):521–528. doi:10.1016/j.ifacol.2016.10.655
[9] Benzerrouk H, Nebylov A, Salhi H. Quadrotor UAV state estimation based on high-degree cubature Kalman filter. IFAC-PapersOnLine. 2016;49(17):349–354. doi:10.1016/j.ifacol.2016.09.060
[10] Huang P, Zhang Z, Luo X, et al. Attitude estimation of agricultural implements based on quaternion and complementary filter. IFAC-PapersOnLine. 2018;51(17):837–842. doi:10.1016/j.ifacol.2018.08.090
[11] Abolhasani M, Rahmani M. Robust deterministic least-squares filtering for uncertain time-varying nonlinear systems with unknown inputs. Syst Control Lett. 2018;122:1–11. doi:10.1016/j.sysconle.2018.09.005
[12] Li X, Chen W, Chan C, et al. Multi-sensor fusion methodology for enhanced land vehicle positioning. Inf Fusion. 2019;46:51–62. doi:10.1016/j.inffus.2018.04.006
[13] Madgwick SO. An efficient orientation filter for inertial and inertial/magnetic sensor arrays. Report x-io Univ Bristol. 2010;25:32. doi:10.1109/ICORR.2011.5975346.
[14] Madgwick SO, Harrison AJ, Vaidyanathan R. Estimation of IMU and MARG orientation using a gradient descent algorithm. IEEE Int Conf Rehabil Robot. 2011;1:1–7.doi:10.1109/ICORR.2011.5975346.
[15] Mansoor S, Bhatti UI, Bhatti AI, et al. Improved attitude determination by compensation of gyroscopic drift by use of accelerometers and magnetometers. Meas J Int Meas Confed. 2019;131:582–589. doi:10.1016/j.measurement.2018.08.067
[16] Alqaisi W, Ghommam J, Alazzam A, et al. Three-loop uncertainties compensator and sliding mode quadrotor control. Comput Electr Eng. 2020;81:106507. doi:10.1016/j.compeleceng.2019.106507
[17] Grassie SL. Measurement of railhead longitudinal profiles: a comparison of different techniques. Wear. 1996;191(1–2):245–251 [4th international conference on contact mechanics and wear of rail–wheel systems]. doi:10.1016/0043-1648(95)06732-9
[18] Chiou S-B, Yen J-Y. Precise railway alignment measurements of the horizontal circular curves and the vertical parabolic curves using the chord method. Proc Inst Mech Eng F J Rail Rapid Transit. 2019;233(5):537–549. doi:10.1177/0954409718800527
[19] Escalona JL, Urda P, Muñoz S. A track geometry measuring system based on multibody kinematics, inertial sensors and computer vision. Sensors. 2021;21(3):683.
[20] Lewis RB. Track-recording techniques used in British rail. IEE Proc B Electr Power Appl. 1984;131:73–81.
[21] Weston P, Roberts C, Yeo G, et al. Perspectives on railway track geometry condition monitoring from in-service railway vehicles. Veh Syst Dyn. 2015;53:1063–1091.
[22] Weston P, Ling CS, Roberts C, et al. Monitoring vertical track irregularity from in-service railway vehicles. Proc Inst Mech Eng F J Rail Rapid Transit. 2007;221(1):75–88.
[23] Weston P, Ling CS, Goodman CJ, et al. Monitoring lateral track irregularity from in-service railway vehicles. Proc Inst Mech Eng F J Rail Rapid Transit. 2007;221(1):89–100.
[24] Seok Lee J, Choi S, Kim S-S, et al. A mixed filtering approach for track condition monitoring using accelerometers on the axle box and bogie. IEEE Trans Instrum Meas. 2012;61:749–758.

[25] Wei X, Liu F, Jia L. Urban rail track condition monitoring based on in-service vehicle acceleration measurements. Measurement. 2016;80:217–228. doi:10.1016/j.measurement.2015.11.033
[26] Tsai HC, Wang CY, Huang NE. Fast inspection and identification techniques for track irregularities based on HHT analysis. Adv Adapt Data Anal. 2012;04(01n02):1250016. doi:10.1142/S1793536912500161
[27] Tsai H-C, Wang C-Y, Huang N, et al. Railway track inspection based on the vibration response to a scheduled train and the Hilbert-Huang transform. Proc Inst Mech Eng F J Rail Rapid Transit. 2015;229(7):815–829. doi:10.1177/0954409714527930
[28] Tsunashima H, Naganuma Y, Kobayashi T. Track geometry estimation from car-body vibration. Veh Syst Dyn. 2014;52:207–219.
[29] De Rosa A, Alfi S, Bruni S. Estimation of lateral and cross alignment in a railway track based on vehicle dynamics measurements. Mech Syst Signal Process. 2019;116:606–623.
[30] Muñoz S, Ros J, Urda P, et al. Estimation of lateral track irregularity using a Kalman filter. experimental validation. J Sound Vib. 2021;504:116122. doi:10.1016/j.jsv.2021.116122
[31] Hartikainen J, Solin A, Särkkä S. Optimal filtering with Kalman filters and smoothers. Department of Biomedical Engineering and Computational Sciences, Aalto University School of Science, 16 August.
[32] Naets F, Cuadrado J, Desmet W. Stable force identification in structural dynamics using Kalman filtering and dummy-measurements. Mech Syst Signal Process. 2015;50–51:235–248.
[33] Brown RG, Hwang PYC. Introduction to random signals and applied Kalman filtering with Matlab exercises. 4th ed. New York: Wiley; 2012.
[34] Queipo NV, Haftka RT, Shyy W, et al. Surrogate-based analysis and optimization. Prog Aerosp Sci. 2005;41(1):1–28.
[35] Urda P, Muñoz S, Aceituno JF, et al. Application and experimental validation of a multibody model with weakly coupled lateral and vertical dynamics to a scaled railway vehicle. Sensors. 2020;20(13):3700.
[36] Miura K. An introduction to maximum likelihood estimation and information geometry. Interdiscipl Inf Sci. 2011;17(3):155–174.
[37] Abbeel P. CS294-40 learning for robotics and control. Kalman filtering, EKF, unscented KF, smoother, EM (Lecture Notes). Berkeley [CA]: University of California; 2008.
[38] Hathaway RJ. A constrained formulation of maximum-likelihood estimation for normal mixture distributions. Ann Stat. 1985;13(2):795–800.
[39] Chatterjee N, Chen Y-H, Maas P, et al. Constrained maximum likelihood estimation for model calibration using summary-level information from external big data sources. J Am Stat Assoc. 2016;111(513):107–117.
[40] EN 13848-5, Railway applications – track – track geometry quality – part 5: geometric quality levels; 2008.

Appendices

Appendix 1: Kalman filter for the orientation and trajectory: matrices of the state space model

This appendix specifies all the expressions required to build the state space model for the Kalman filter. Parameter Δt represents the sampling interval.

$$\begin{Bmatrix} \boldsymbol{x}_{k+1} = \mathbf{F}\boldsymbol{x}_k + \boldsymbol{q}_k \\ \boldsymbol{z}_k = \mathbf{g}(\boldsymbol{x}_k) + \boldsymbol{u}_k \end{Bmatrix} \quad \text{with} \quad \begin{Bmatrix} \boldsymbol{q}_k \sim \mathbf{N}(\mathbf{0}, \mathbf{Q}) \\ \boldsymbol{u}_k \sim \mathbf{N}(\mathbf{0}, \mathbf{U}) \end{Bmatrix},$$

$$\boldsymbol{z} = \begin{bmatrix} \omega_x^{imu} & \omega_y^{imu} & \omega_z^{imu} & a_x^{imu} & a_y^{imu} & a_z^{imu} & 0 & \delta \end{bmatrix}^{\mathrm{T}},$$

$$\boldsymbol{x} = \begin{bmatrix} \varphi^b & \dot{\varphi}^b & \theta^b & \dot{\theta}^b & \psi^b & \dot{\psi}^b & r_y^{t,b} & \dot{r}_y^{t,b} & \ddot{r}_y^{t,b} & r_z^{t,b} & \dot{r}_z^{t,b} & \ddot{r}_z^{t,b} \end{bmatrix}^{\mathrm{T}},$$

$$\mathbf{F} = \begin{bmatrix} \mathbf{F}_1 & \mathbf{0} & \mathbf{0} & \mathbf{0} & \mathbf{0} \\ \mathbf{0} & \mathbf{F}_1 & \mathbf{0} & \mathbf{0} & \mathbf{0} \\ \mathbf{0} & \mathbf{0} & \mathbf{F}_1 & \mathbf{0} & \mathbf{0} \\ \mathbf{0} & \mathbf{0} & \mathbf{0} & \mathbf{F}_2 & \mathbf{0} \\ \mathbf{0} & \mathbf{0} & \mathbf{0} & \mathbf{0} & \mathbf{F}_2 \end{bmatrix},$$

$$\mathbf{F}_1 = \begin{bmatrix} 1 & \Delta t \\ 0 & 1 \end{bmatrix}, \quad \mathbf{F}_2 = \begin{bmatrix} 1 & \Delta t & \Delta t^2/2 \\ 0 & 1 & \Delta t \\ 0 & 0 & 1 \end{bmatrix},$$

$$\mathbf{g}(\boldsymbol{x}) = \begin{bmatrix} \dot{\varphi}^b - \theta^b \dot{\psi}^b \\ \dot{\theta}^b + \varphi^b \dot{\psi}^b \\ \dot{\psi}^b - \varphi^b \dot{\theta}^b \\ \mathrm{g}_{4A}(\boldsymbol{x}) + \mathrm{g}_{4B}(\boldsymbol{x}) + \mathrm{g}_{4C}(\boldsymbol{x}) + \mathrm{g}_{4D}(\boldsymbol{x}) + \mathrm{g}_{4E}(\boldsymbol{x}) \\ \mathrm{g}_{5A}(\boldsymbol{x}) + \mathrm{g}_{5B}(\boldsymbol{x}) + \mathrm{g}_{5C}(\boldsymbol{x}) + \mathrm{g}_{5D}(\boldsymbol{x}) + \mathrm{g}_{5E}(\boldsymbol{x}) \\ \mathrm{g}_{6A}(\boldsymbol{x}) + \mathrm{g}_{6B}(\boldsymbol{x}) + \mathrm{g}_{6C}(\boldsymbol{x}) + \mathrm{g}_{6D}(\boldsymbol{x}) + \mathrm{g}_{6E}(\boldsymbol{x}) \\ r_y^{t,b} \\ r_z^{t,b} \end{bmatrix},$$

$$\mathrm{g}_{4A}(\boldsymbol{x}) = \left(V^2(\rho_{tw}\rho_v - \rho_h') - \rho_h \dot{V} - (\psi^b - \psi^t)V^2(\rho_{tw}^2 + \rho_h^2) - (\theta^b - \theta^t)(\rho_v\rho_h V^2 + \rho_{tw}\dot{V})\right) r_y^{t,b},$$

$$\mathrm{g}_{4B}(\boldsymbol{x}) = \left(-2\rho_h V - 2\rho_{tw}V(\theta^b - \theta^t)\right) \dot{r}_y^{t,b} + (\psi^b - \psi^t)\ddot{r}_y^{t,b},$$

$$\mathrm{g}_{4C}(\boldsymbol{x}) = \left(\rho_v \dot{V} + \rho_{tw}\rho_h V^2 + (\psi^b - \psi^t)(\rho_v\rho_h V^2 - \rho_{tw}\dot{V}) + (\theta^b - \theta^t)(\rho_{tw}^2 + \rho_h^2)V^2\right) r_z^{t,b},$$

$$\mathrm{g}_{4D}(\boldsymbol{x}) = \left(2\rho_v V - 2(\psi^b - \psi^t)\rho_{tw}V\right) \dot{r}_z^{t,b} - (\theta^b - \theta^t)\ddot{r}_z^{t,b},$$

$$\mathrm{g}_{4E}(\boldsymbol{x}) = -g\theta^b + (\psi^b - \psi^t)\rho_h V^2 + (\theta^b - \theta^t)\rho_v V^2 + \dot{V},$$

$$\mathrm{g}_{5A}(\boldsymbol{x}) = \Big((\psi^t - \psi^b)\left(V^2(\rho_{tw}\rho_v - \rho_h') - \rho_h \dot{V}\right) - V^2(\rho_{tw}^2 + \rho_h^2) + (\varphi^b - \varphi^t)(\rho_v\rho_h V^2 + \rho_{tw}\dot{V})\Big) r_y^{t,b},$$

$$\mathrm{g}_{5B}(\boldsymbol{x}) = \left(2\rho_h V(\psi^b - \psi^t) + 2\rho_{tw}V(\varphi^b - \varphi^t)\right) \dot{r}_y^{t,b} + \ddot{r}_y^{t,b},$$

$$\mathrm{g}_{5C}(\boldsymbol{x}) = \left((\psi^t - \psi^b)(\rho_v \dot{V} + \rho_{tw}\rho_h V^2) + \rho_v\rho_h V^2 - \rho_{tw}\dot{V} - V^2(\varphi^b - \varphi^t)(\rho_{tw}^2 + \rho_h^2)\right) r_z^{t,b},$$

$$\mathrm{g}_{5D}(\boldsymbol{x}) = \left(2\rho_v V(\psi^t - \psi^b) - 2\rho_{tw}V\right) \dot{r}_z^{t,b} + (\varphi^b - \varphi^t)\ddot{r}_z^{t,b},$$

$$\mathrm{g}_{5E}(\boldsymbol{x}) = g\varphi^b + (\psi^t - \psi^b)\dot{V} + (\varphi^t - \varphi^b)\rho_v V^2 + \rho_h V^2,$$

$$\mathrm{g}_{6A}(\boldsymbol{x}) = \left((\theta^b - \theta^t)\left(V^2(\rho_{tw}\rho_v - \rho_h') - \rho_h \dot{V}\right) + (\varphi^b - \varphi^t)V^2(\rho_{tw}^2 + \rho_h^2) + \rho_v\rho_h V^2 + \rho_{tw}\dot{V}\right) r_y^{t,b},$$

$$\mathrm{g}_{6B}(\boldsymbol{x}) = \left(2\rho_h V(\theta^t - \theta^b) + 2\rho_{tw}V\right) \dot{r}_y^{t,b} + (\varphi^t - \varphi^b)\ddot{r}_y^{t,b},$$

$$\mathrm{g}_{6C}(\boldsymbol{x}) = \left((\theta^b - \theta^t)(\rho_v \dot{V} + \rho_{tw}\rho_h V^2) + (\varphi^t - \varphi^b)(\rho_v\rho_h V^2 - \rho_{tw}\dot{V}) - V^2(\rho_{tw}^2 + \rho_h^2)\right) r_z^{t,b},$$

$$\mathrm{g}_{6D}(\boldsymbol{x}) = \left(2(\theta^b - \theta^t)\rho_v V + 2(\varphi^b - \varphi^t)\rho_{tw}V\right) \dot{r}_z^{t,b} + \ddot{r}_z^{t,b},$$

$$\mathrm{g}_{6E}(\boldsymbol{x}) = (\theta^b - \theta^t)\dot{V} + (\varphi^t - \varphi^b)\rho_h V^2 - \rho_v V^2 + g,$$

$$\mathbf{J} = \frac{\partial \mathbf{g}}{\partial \boldsymbol{x}} = \begin{bmatrix} 0 & 1 & -\dot{\psi}^b & 0 & 0 & -\dot{\theta}^b & 0 & 0 & 0 & 0 & 0 & 0 \\ \dot{\psi}^b & 0 & 0 & 1 & 0 & \varphi^b & 0 & 0 & 0 & 0 & 0 & 0 \\ -\dot{\theta}^b & 0 & 0 & -\varphi^b & 0 & 1 & 0 & 0 & 0 & 0 & 0 & 0 \\ 0 & 0 & J_{4,3} & 0 & J_{4,5} & 0 & J_{4,7} & J_{4,8} & J_{4,9} & J_{4,10} & J_{4,11} & J_{4,12} \\ J_{5,1} & 0 & 0 & 0 & J_{5,5} & 0 & J_{5,7} & J_{5,8} & J_{5,9} & J_{5,10} & J_{5,11} & J_{5,12} \\ J_{6,1} & 0 & J_{6,3} & 0 & 0 & 0 & J_{6,7} & J_{6,8} & J_{6,9} & J_{6,10} & J_{6,11} & J_{6,12} \\ 0 & 0 & 0 & 0 & 0 & 0 & 1 & 0 & 0 & 0 & 0 & 0 \\ 0 & 0 & 0 & 0 & 0 & 0 & 0 & 0 & 0 & 1 & 0 & 0 \end{bmatrix},$$

$$\begin{aligned}
J_{4,3} &= -r_y^{t,b}(\rho_v\rho_h V^2 + \rho_{tw}\dot{V}) - 2\rho_{tw}V\dot{r}_y^{t,b} + r_z^{t,b}V^2(\rho_{tw}^2 + \rho_h^2) - \ddot{r}_z^{t,b} - g + \rho_v V,\\
J_{4,5} &= -r_y^{t,b}V^2(\rho_{tw}^2 + \rho_h^2) + \ddot{r}_y^{t,b} + r_z^{t,b}(\rho_v\rho_h V^2 - \rho_{tw}\dot{V}) - 2\rho_{tw}V\dot{r}_z^{t,b} + \rho_h V^2,\\
J_{4,7} &= V^2(\rho_{tw}\rho_v - \rho_h') - \rho_h\dot{V} + (\psi^t - \psi^b)V^2(\rho_{tw}^2 + \rho_h^2) + (\theta^t - \theta^b)(\rho_v\rho_h V^2 + \rho_{tw}\dot{V}),\\
J_{4,8} &= -2\rho_h V - 2\rho_{tw}V(\theta^b - \theta^t),\\
J_{4,9} &= \psi^b - \psi^t,\\
J_{4,10} &= \rho_v\dot{V} + \rho_{tw}\rho_h V^2 + (\psi^b - \psi^t)(\rho_v\rho_h V^2 - \rho_{tw}\dot{V}) + (\theta^b - \theta^t)(\rho_{tw}^2 + \rho_h^2)V^2,\\
J_{4,11} &= 2\rho_v V + 2(\psi^t - \psi^b)\rho_{tw}V,\\
J_{4,12} &= \theta^t - \theta^b,\\
J_{5,1} &= (\rho_v\rho_h V^2 + \rho_{tw}\dot{V})r_y^{t,b} + 2\rho_{tw}V\dot{r}_y^{t,b} - V^2(\rho_{tw}^2 + \rho_h^2)r_z^{t,b} + \ddot{r}_z^{t,b} + g - \rho_v V^2,\\
J_{5,5} &= \left(\rho_h\dot{V} - V^2(\rho_{tw}\rho_v - \rho_h')\right)r_y^{t,b} + 2\rho_h V\dot{r}_y^{t,b} - (\rho_v\dot{V} + \rho_{tw}\rho_h V^2)r_z^{t,b} - 2\rho_v V\dot{r}_z^{t,b} - \dot{V},\\
J_{5,7} &= (\psi^t - \psi^b)\left(V^2(\rho_{tw}\rho_v - \rho_h') - \rho_h\dot{V}\right) - V^2(\rho_{tw}^2 + \rho_h^2) + (\varphi^b - \varphi^t)(\rho_v\rho_h V^2 + \rho_{tw}\dot{V}),\\
J_{5,8} &= 2\rho_h V(\psi^b - \psi^t) + 2\rho_{tw}V(\varphi^b - \varphi^t),\\
J_{5,9} &= 1,\\
J_{5,10} &= (\psi^t - \psi^b)(\rho_v\dot{V} + \rho_{tw}\rho_h V^2) + \rho_v\rho_h V^2 - \rho_{tw}\dot{V} + V^2(\varphi^t - \varphi^b)(\rho_{tw}^2) + \rho_h^2,\\
J_{5,11} &= 2\rho_v V(\psi^t - \psi^b) - 2\rho_{tw}V,\\
J_{5,12} &= \varphi^b - \varphi^t,\\
J_{6,1} &= V^2(\rho_{tw}^2 + \rho_h^2)r_y^{t,b} + \ddot{r}_y^{t,b} + (\rho_{tw}\dot{V} - \rho_v\rho_h V^2)r_z^{t,b} + 2\rho_{tw}V\dot{r}_z^{t,b} - \rho_h V^2,\\
J_{6,3} &= \left(V^2(\rho_{tw}\rho_v - \rho_h') - \rho_h\dot{V}\right)r_y^{t,b} - 2\rho_h V\dot{r}_y^{t,b} + (\rho_v\dot{V} + \rho_{tw}\rho_h V^2)r_z^{t,b} + 2\rho_v V\dot{r}_z^{t,b} + \dot{V},\\
J_{6,7} &= (\theta^b - \theta^t)\left(V^2(\rho_{tw}\rho_v - \rho_h') - \rho_h\dot{V}\right) + (\varphi^b - \varphi^t)V^2(\rho_{tw}^2 + \rho_h^2) + \rho_v\rho_h V^2 + \rho_{tw}\dot{V},\\
J_{6,8} &= 2\rho_h V(\theta^t - \theta^b) + 2\rho_{tw}V,\\
J_{6,9} &= \varphi^t - \varphi^b,\\
J_{6,10} &= (\theta^b - \theta^t)(\rho_v\dot{V} + \rho_{tw}\rho_h V^2) + (\varphi^t - \varphi^b)(\rho_v\rho_h V^2 - \rho_{tw}\dot{V}) - V^2(\rho_{tw}^2 + \rho_h^2),\\
J_{6,11} &= 2(\theta^b - \theta^t)\rho_v V + 2(\varphi^b - \varphi^t)\rho_{tw}V,\\
J_{6,12} &= 1,
\end{aligned}$$

$$\mathbf{Q} = \begin{bmatrix} q_\varphi \mathbf{Q}_1 & \mathbf{0} & \mathbf{0} & \mathbf{0} & \mathbf{0} \\ \mathbf{0} & q_\theta \mathbf{Q}_1 & \mathbf{0} & \mathbf{0} & \mathbf{0} \\ \mathbf{0} & \mathbf{0} & q_\psi \mathbf{Q}_1 & \mathbf{0} & \mathbf{0} \\ \mathbf{0} & \mathbf{0} & \mathbf{0} & q_y \mathbf{Q}_2 & \mathbf{0} \\ \mathbf{0} & \mathbf{0} & \mathbf{0} & \mathbf{0} & q_z \mathbf{Q}_2 \end{bmatrix},$$

$$\mathbf{Q}_1 = \begin{bmatrix} \Delta t^3/3 & \Delta t^2/2 \\ \Delta t^2/2 & \Delta t \end{bmatrix}, \quad \mathbf{Q}_2 = \begin{bmatrix} \Delta t^5/20 & \Delta t^4/8 & \Delta t^3/6 \\ \Delta t^4/8 & \Delta t^3/3 & \Delta t^2/2 \\ \Delta t^3/6 & \Delta t^2/2 & \Delta t \end{bmatrix},$$

$$\mathbf{U} = \begin{bmatrix} u_x^\omega & 0 & 0 & 0 & 0 & 0 & 0 & 0 \\ 0 & u_y^\omega & 0 & 0 & 0 & 0 & 0 & 0 \\ 0 & 0 & u_z^\omega & 0 & 0 & 0 & 0 & 0 \\ 0 & 0 & 0 & u_x^{ac} & 0 & 0 & 0 & 0 \\ 0 & 0 & 0 & 0 & u_y^{ac} & 0 & 0 & 0 \\ 0 & 0 & 0 & 0 & 0 & u_z^{ac} & 0 & 0 \\ 0 & 0 & 0 & 0 & 0 & 0 & u_y^{pos} & 0 \\ 0 & 0 & 0 & 0 & 0 & 0 & 0 & u_z^{pos} \end{bmatrix}.$$

Appendix 2: Results: track irregularity profiles

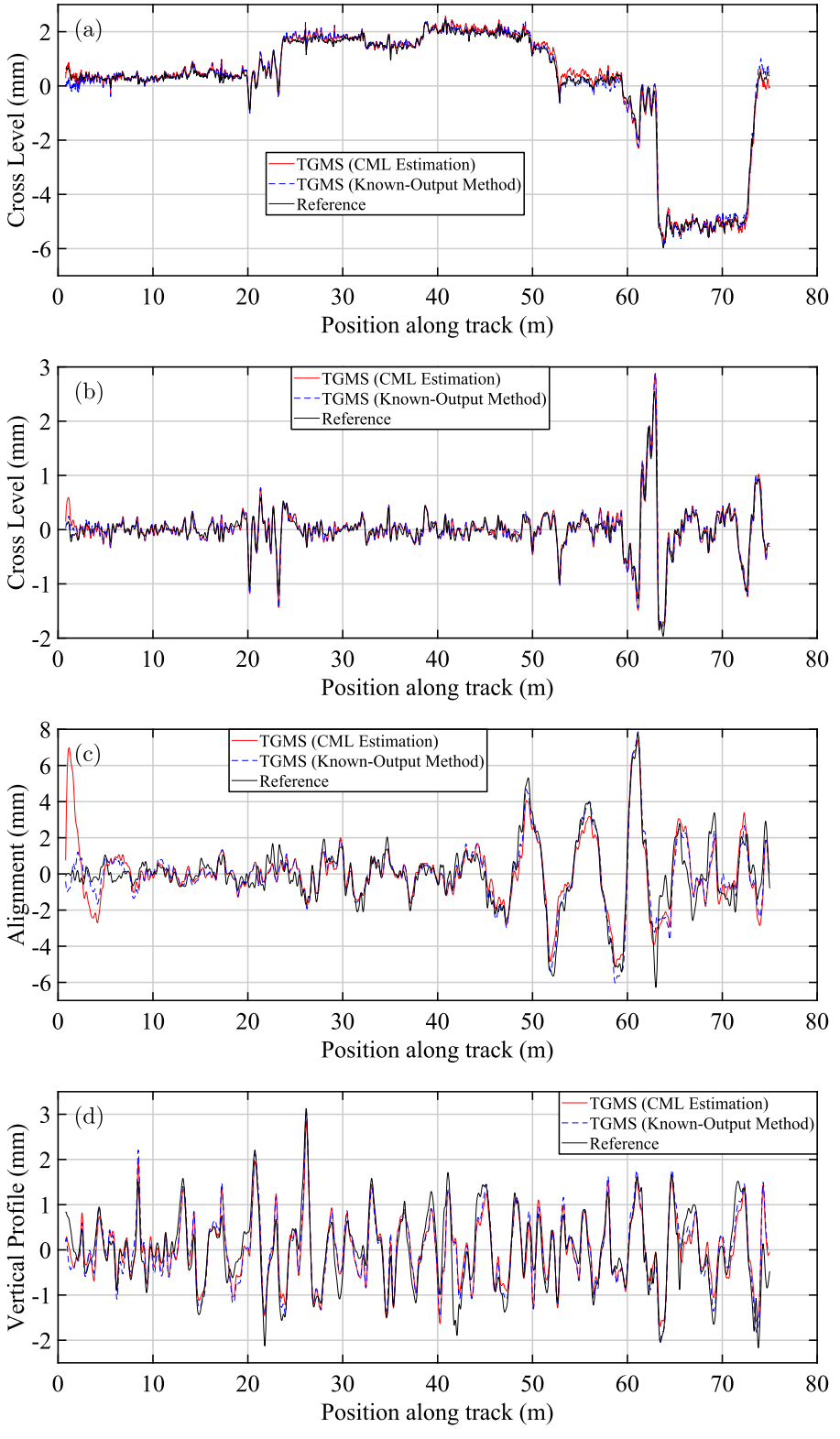

Figure A1. Irregularities obtained with the TGMS (either using CML estimation or KOM), compared to the reference irregularities. (a) Unfiltered and (b–d) filtered.

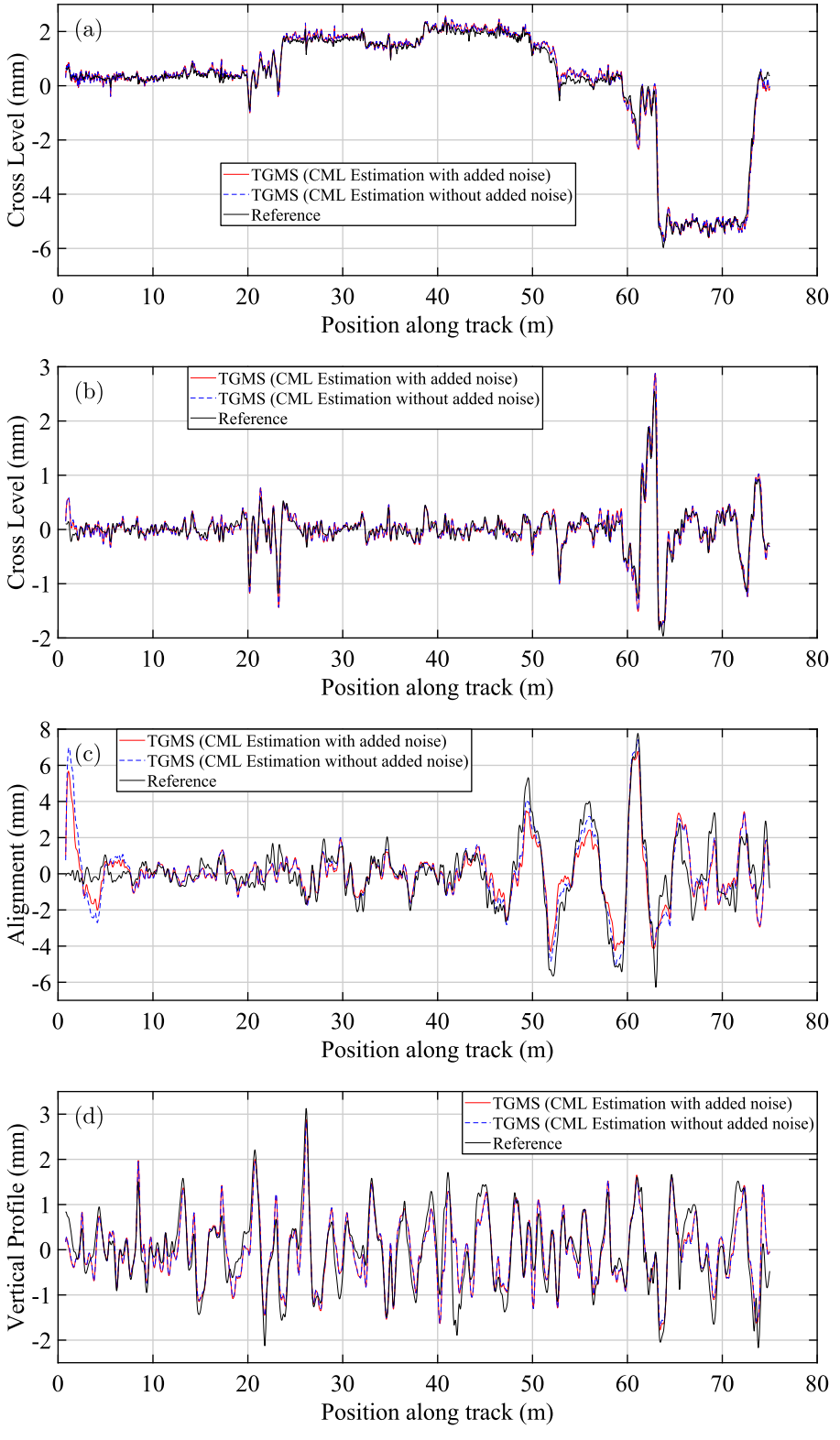

Figure A2. Irregularities obtained using CML estimation (with and without artificial noise on the IMU signals), compared to the reference irregularities. (a) Unfiltered and (b–d) filtered.

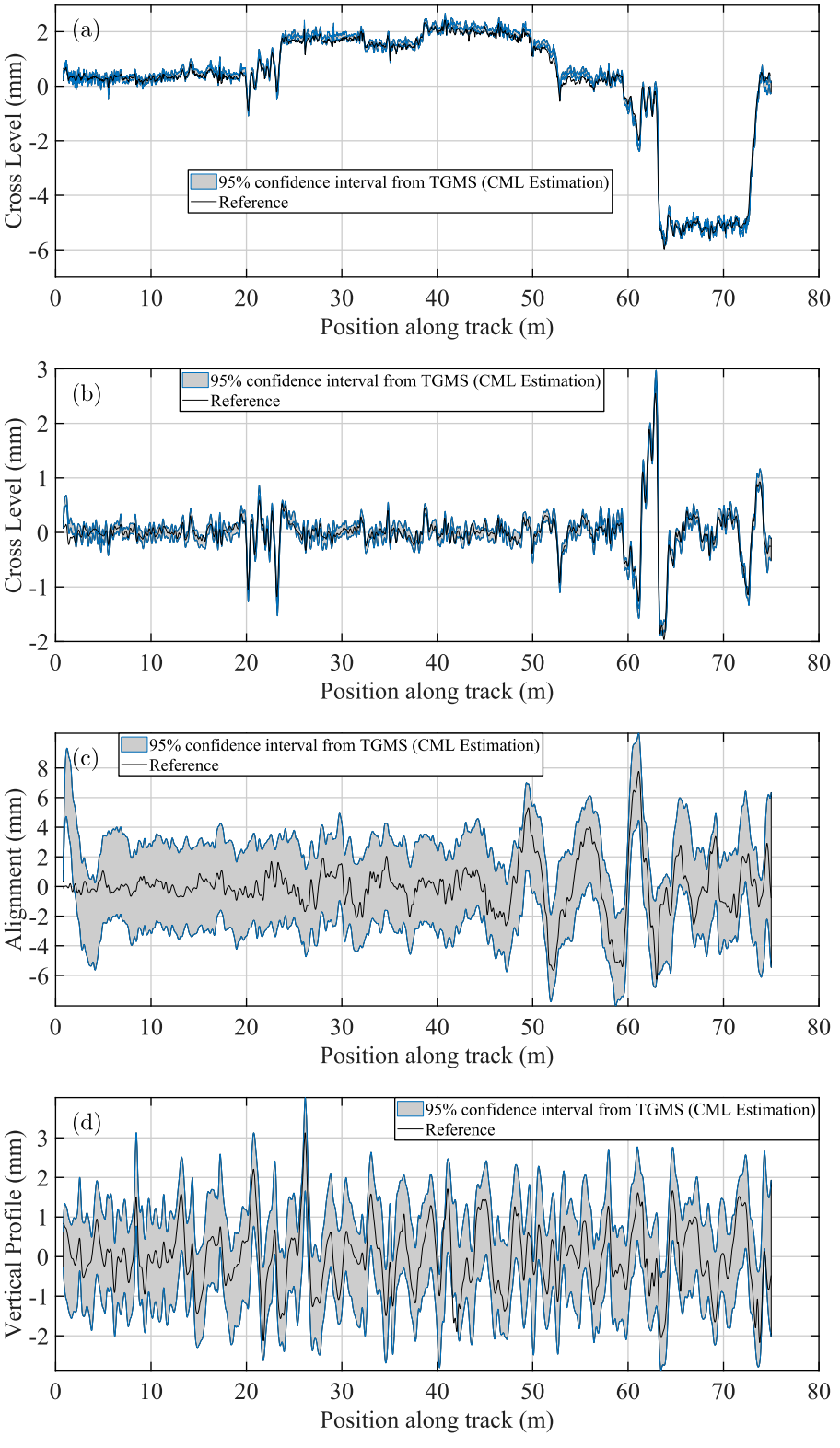

Figure A3. 95% confidence intervals for the different irregularities obtained with CML estimation, compared to the reference irregularities. (a) Unfiltered and (b–d) filtered.